N2O dissociation on small Rh clusters: A density functional study P.L. Rodríguez-Kessler a, A.R. Rodríguez-Domínguez Computational Materials Science 97 (2015) 32–35

1 AUTHOR:

Adán Rubén Rodríguez Domínguez
Universidad Autónoma de San Luis Potosí
25 PUBLICATIONS **18** CITATIONS

N$_2$O dissociation on small Rh clusters: A density functional study

P.L. Rodríguez-Kessler [a], A.R. Rodríguez-Domínguez [b],*

[a] Intituto Potosino de Investigación Científica y Tecnológica, Camino a la presa San José 2055, San Luis Potosí 78216, Mexico
[b] Instituto de Física, Universidad Autónoma de San Luis Potosí, San Luis Potosí 78000, Mexico

ARTICLE INFO

ABSTRACT

Density functional theory calculations are performed on Rh$_{1-6}$ clusters to study N$_2$O adsorption and dissociation as a model for the N$_2$O decomposition reaction. For Rh$_{1-6}$N$_2$O clusters the molecular precursor adsorptions are found to occur at the bridge sites and on certain top sites. For all clusters, N$_2$O decomposition initiated by N–O bond breaking is more favorable to form N$_2$ and O as the final products. Dissociative adsorptions are energetically prefered for Rh$_{1-6}$N$_2$O clusters and the adsorption energy increases with cluster size. The N$_2$O dissociation process involves a small barrier for Rh$_{1-4}$ clusters, and it is found barrierless, for dissociations on Rh$_{5-6}$ clusters. The relevant magnetic moments of the Rh$_{1-6}$ clusters interacting with N$_2$O are discussed. For comparison when going to larger clusters, we have also calculated the N$_2$O dissociation taking place on the Rh(1 1 1) surface. We found that both on the Rh clusters as well as on the Rh(1 1 1) surface the N$_2$O catalytic dissociation is possible.

© 2014 Elsevier B.V. All rights reserved.

1. Introduction

Recent experiments have shown that Rh is an active catalyst for different reactions in environmental chemistry such as CO oxidation [1], benzene dehydrogenation [2], and NO$_x$ decomposition [3–5], as well as in the reduction of harmful gases. That is why we are now analyzing these Rh catalytic properties from a theoretical viewpoint.

Since the 1970s acid rain has been manifested to mankind by its harmful effects to flora and ecology in general, due as a result of the huge industrial sulfur dioxide emissions into the atmosphere, which convert into sulfuric acid. Since then, many efforts have been undertaken to diminish this type of emissions. However, little has been done to counteract the other type of acid rain which is caused by the presence of nitric acid in the atmosphere, generated by the nitrous oxide N$_2$O emissions [6], which appear not only from industrial but also from agriculture activities, fossil fuel combustion, biomass and biofuel burning, and a few other processes [7]. It is also to be pointed out that nitrous oxide is a powerful greenhouse gas whose effects are as bigger as a factor of three hundred compared with carbon dioxide [8,9]. As nobody is until now contraresting the increasing emissions of nitrous dioxide, whose molecule stability and lifetime in the atmosphere is estimated of over hundred years, and its presence turns out to be as undesirable and dangerous, as it is also considered, that it will be the main responsible of the ozone depletion in the atmosphere during the whole present 21st century, besides the fluorochlorocarbons which have been put already under control, it is now time to identify a candidate for a catalytic device or procedure to avoid nitrous oxide emissions in the atmosphere.

A first step in the understanding of the catalytic activity for the N$_2$O decomposition reaction, requires the knowledge of the energetically most stable adsorption sites of the reactant and products and the most favorable decomposition reaction pathways [10]. In this contribution, we systematically investigate the interaction between N$_2$O and Rh$_{1-6}$ clusters using the first principles methods on the basis of DFT. In order to determine the evolution of size and structural effects on the catalytic activity for N$_2$O decomposition, we calculate both molecular and dissociative adsorptions as well as the energy barriers to obtain N$_2$ and atomic O as the final products. This article is organized as follows. In Section 2 we briefly describe the details of the computational methodology. In Section 3 we present the main results of our calculations for Rh$_{1-6}$ clusters interacting with N$_2$O. Finally, in Section 4 the summary of our main findings and conclusions are given.

2. Methods

2.1. For the Rh clusters

The calculations we report in this work are based in the framework of Kohn–Sham (KS) density-functional theory [11], implemented by the code Vienna ab initio simulation package (VASP) [12,13]. The exchange and correlation (XC) energy-functional is treated using a generalized gradient approximation (GGA)

Table 1
Properties of the Rh_n bare clusters.

Rh_n	Symmetry	$E_B/atom$ (eV/atom)	Rh–Rh (Å)	μ_T (μ_B)
2	D_{2h}	1.80	2.21	4
3	D_{3h}	2.38	2.37	3
4	T_d	2.73	2.44	0
5	C_{4v}	3.09	2.42–2.53	5
6	O_h	3.26	2.54–2.54	6

developed by Perdew–Burke–Ernzerhof (PBE) [14]. The interactions between ions and electrons are described using the projector-augmented-wave (PAW) method [15]. The $5s^1 4d^8$ orbitals of Rh, and the $2s^2 2p^4$ of O, and the $2s^2 2p^3$ of N are treated as valence states. The Kohn–Sham one-electron valence states were expanded in a basis of plane waves with a kinetic energy cutoff of 375 eV. A Gaussian smearing of $\sigma = 0.01$ eV was used for all calculations to improve convergence. Only the Γ point is taken into account to represent the Brillouin zone and a cubic supercell of $16 \times 16 \times 16$ Å was used to avoid the interaction between periodic images. The cluster geometries were determined by decorating the Rh_{1-6} ground state structures with a N_2O molecule. The atomic positions are relaxed selfconsistently without restrictions in the symmetry by the conjugated-gradient algorithm with a convergence criteria of 10^{-6} eV of the total energy change and 0.01 eV/Å for the forces acting on all atoms. The Rh(1 1 1) surface

was modeled by a four-layer slab with a $(2\sqrt{3} \times 4)$ surface unit cell, separated by 12 Å of vacuum with all layers fully relaxed. A Monkhorst–Pack k-point sampling [16] was performed using a $4 \times 4 \times 1$ grid. A Fermi broadening of 0.2 eV was applied. Using the present setup the lattice constant of Rh bulk is found to be 3.845 Å in close agreement with experimental and previous theoretical results [17,18]. The adsorption energy is calculated by the expression
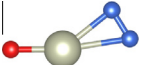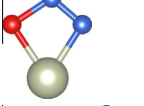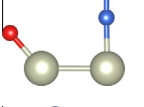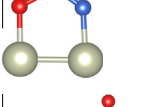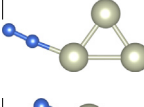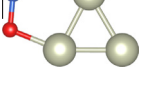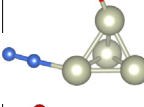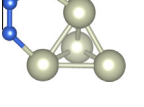
$$E_{ad} = E(Rh_n N_2 O) - E(Rh_n) - E(N_2 O),$$

where $E(Rh_n N_2 O)$, $E(Rh_n)$ and $E(N_2 O)$ are the total energies of the $Rh_n N_2 O$ complex, and the noninteracting fragments Rh_n and $N_2 O$, respectively. A negative E_{ad} value corresponds to a stable adsorption. In order to calculate the activation energy E_{Act} for $N_2 O$ dissociation, the transition state (TS) of $Rh_n N_2 O$ is located using the dimer method [19]. The local atomic charges are calculated following the atoms in molecules approach by using the numerical algorithm developed by Henkelman et al. [20].
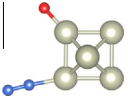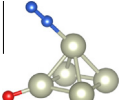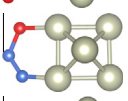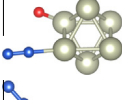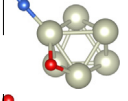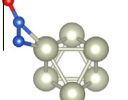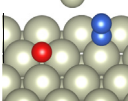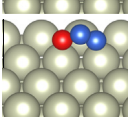
2.2. For the Rh(1 1 1) surface

The Rh(1 1 1) surface was modeled by a four-layer slab with a $(2\sqrt{3} \times 4)$ surface unit cell, separated by 12 Å of vacuum with all layers fully relaxed. A Monkhorst–Pack k-point sampling [16] was performed using a $4 \times 4 \times 1$ grid. A Fermi broadening of 0.2 eV was applied. Using the present setup the lattice constant

Table 2
Structures of $Rh_{2-6}N_2O$ complexes. The total magnetic moment μ_T, adsorption energy E_{ad}, O–N, Rh–N bond distances and the N_2O Bader charge are given for the lowest energy configurations.

		μ_T (μ_B)	E_{ad} (eV)	d_{N-O} (Å)	d_{Rh-O} (Å)	qN_2O (e)
	1a	1	−2.66		1.75	−1.08
		3	−2.87		1.76	−0.93
	1b	1	−1.22	1.46	1.97	−0.75
		3	−0.37	1.38	2.14	−0.67
	2a	0	−2.20		1.73	−0.95
		2	−2.34		1.73	−0.98
	2b	2	−1.20	1.44	1.90	−0.81
		4	−0.87	1.35	2.08	−0.78
	3a	1	−2.82		1.71	−0.99
		3	−2.68		1.73	−0.97
	3b	3	−0.93	1.33	2.05	−0.76
		5	−0.88	1.36	2.06	−0.81
	4a	0	−3.15		1.71	−1.03
		2	−2.95		1.74	−1.02
		4	−2.79		1.73	−1.00
	4b	0	−1.12	1.36	2.01	−0.79
		2	−1.10	1.38	1.98	−0.79
		4	−1.16	1.37	2.00	−0.80

Table 3
Structures of $Rh_{2-6}N_2O$ and on the Rh(111) surface complexes. The total magnetic moment μ_T, adsorption energy E_{ad}, O–N, Rh–N bond distances and the N_2O Bader charge are given for the lowest energy configurations.

		μ_T (μ_B)	E_{ad} (eV)	d_{N-O} (Å)	d_{Rh-O} (Å)	q_{N_2O} (e)
	5a	1	−3.18		1.73	−1.01
		3	−3.14		1.73	−1.01
		5	−3.08		1.74	−0.99
	5b	3	−3.09		1.74	−1.00
	5c	7	−1.20	1.42	1.99	−0.84
	6a	0	−3.28		1.73	−1.03
		2	−3.26		1.73	−1.03
		4	−3.27		1.74	−1.02
	6b	6	−3.11		1.95	−1.13
	6c	6	−0.97	1.24	3.13	−0.61
	Rh(111)a	0	−2.62		2.15	−1.07
	Rh(111)b	0	−0.19	1.39	2.19	−0.66

of fcc bulk of Rh is found to be 3.845 Å in close agreement with experimental and previous theoretical results [17,18].

3. Results

3.1. Bare Rh_n (n = 1–6) clusters

We found that the ground state of the Rh monomer has a total magnetic moment of $\mu_T = 2\ \mu_B$ due to the eight electrons filling the 4d magnetic shell. In agreement with previous theoretical calculations (DFT [21,22]), the ground state of the rhodium dimer has 4 μ_B with a bond distance of 2.21 Å. The calculated properties of Rh_{2-6} clusters are summarized in Table 1. The average binding energy is calculated by the formula

$$E_B/atom = [nE(Rh) - E(Rh_n)]/n,$$

for each cluster. Our calculations show that for Rh_3, the triangular geometry is more stable to the linear geometry ($D_{\infty h}$). Compact structures Rh_n, (n = 4–6) are more stable than open structures.

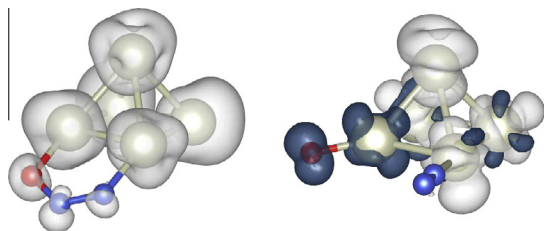### 3.2. Rh_nN_2O adsorption complexes

In Tables 2 and 3 the structural and energetic profiles for the most stable $Rh_{1-6}N_2O$ adsorbed complexes are presented. Lower case letters (a, b, c, etc.) are used to label the complexes for a given size in order of decreasing stability. In the following discussion, we present the results of the N_2O adsorptions for each cluster separately.

Rh_1N_2O. In the ground state the N_2O molecule has a linear structure with 0 μ_B. The N–O bond distance is 1.20 Å and the N–N bond distance is 1.14 Å, respectively. When it approaches to the Rh monomer during the relaxation process, the N_2O molecule is adsorbed as a molecular precursor state (see structure 1b in Table 2). It forms an O–N–N angle of 105.8° with −1.22 eV of adsorption energy and $\mu_T = 1\ \mu_B$. The O–N and N–N bond distances (1.46 Å and 1.24 Å) are elongated compared to the bare N_2O molecule. In order to determine the N_2O molecule dissociation step, the TS for both N–O and N–N dissociations were calculated using the dimer method approach, it results that the N–N dissociation path is not energetically favorable for all cases considered. The TS of the 1a complex has a breaking N–O bond distance of 1.67 Å and a small energy barrier of 0.04 eV. After dissociation (1a) the dissociative adsorption (DA) results more favorable than the molecular adsorption (MA). The adsorption energy is −2.87 eV and the total magnetic moment increases to 3 μ_B.

Rh_2N_2O. For the Rh dimer the DA is energetically favoured. The adsorption energy is −2.34 eV with an energy barrier of 0.27 eV. The most stable molecular precursor state (2b complex) has 1.14 eV less adsorption energy, with a bridge adsorption having 2 μ_B of total magnetic moment. The O–N and N–N bond distances are 1.44 Å and 1.22 Å, respectively.

Rh_3N_2O. The most stable complex, 3a, has a bridge DA with −2.82 eV of adsorption energy and 1 μ_B. The calculated energy barrier is 0.04 eV. The energetically best MA complex (3b) has −0.93 eV of adsorption energy and 3 μ_B. The bond distances are $d_{N--O} = 1.33$ Å and $d_{N--N} = 1.21$ Å for the N_2O adsorbed molecule. Remarkably, for a given MA, the N–O bond is typically more elongated.

Fig. 1. Isosurface of the local spin polarization (i.e., the local difference between the spin-up and spin-down electron densities) of 5c (left) and 5a (right) complexes.

Rh_4N_2O. The ground state structure of 4a is a DA with -3.15 eV of adsorption energy. The energy barrier is 0.08 eV and the magnetic moment is 0 μ_B. The most stable MA (4b) has 4 μ_B with -1.16 eV of adsorption energy. The Bader population analysis indicates that electrons are transferred from Rh_n clusters to the adsorbates. Besides the negative charge on N_2O (see in Tables 2 and 3) it increases with the cluster size, which is consistent with the trend of the adsorption energies.

Rh_5N_2O. The ground state structure of the bare Rh_5 cluster consists of a tetragonal pyramid with 5 μ_B. Here, N_2O has a barrierless dissociation on both unequivalent bridge sites of the Rh_5 cluster. The final structure corresponds to a DA with 1 μ_B and -3.18 eV of adsorption energy. Two molecular precursor states are located on this cluster. 5c has a bridge site adsorption with -1.20 eV of adsorption energy, interestingly the magnetic moment increases from 5 μ_B to 7 μ_B. In Fig. 1 the spin polarization of the 5c complex shows that the N_2O molecule has a ferromagnetic-like coupling on the Rh_5 cluster. For the DA (5a), the oxygen atom performs an anti-ferromagnetic-like coupling and the total magnetic moment is decreased. In the 5d complex (not shown) the N_2O molecule adsorbs upsidedown on the top site. However, the adsorption energy is relatively small (-0.82 eV) and the magnetic moment remains unchanged (5 μ_B) due to the small interaction.

Rh_6N_2O. The ground state structure of the bare Rh_6 cluster is a D_{4h} tetragonal bipyramid with an average bond distance of 2.54 Å and 6 μ_B. It has only 3 different adsorption sites (top, bridge, hollow) due to the O_h symmetry. Interestingly, the N_2O molecule performs dissociative adsorptions without any evident barrier on the bridge site. The most stable 6a complex has 0 μ_B and -3.28 eV of adsorption energy. Another DA adsorption (6b) is 0.17 eV lower in adsorption energy and it is formed when the N_2O molecule is horizontally adsorbed on the Rh top site. The 6c complex is the molecularly most stable adsorption with both nitrogen atoms bonded on top.

The results presented here provide insight into the initial steps involved in the N_2O dissociation over Rh_N. The activation barriers show that the dissociation reactions on these Rh_{1-6} clusters are expected to occur more rapidly compared to those on larger clusters. We show this in the next subsection where we discuss the N_2O dissociation process on the Rh surface.

3.3. N_2O adsorption on the Rh surface

The results of N_2O adsorption on the Rh(1 1 1) surface have been also listed in Table 3 for comparison. Our results for the Rh(1 1 1) surface show that the deepest MA occurs on the bridge site with an adsorption energy of $E_{ad} = -0.19$ eV, which in Table 3 is labeled as Rh(1 1 1)b. The energy barrier for N_2O dissociation on the Rh(1 1 1) surface amounts to $E_{Act} = 0.35$ eV, slightly larger than E_{ad}. There is here a challenge for the experimentalists how to induce a tunneling into the dissociated state without losing the

N_2O molecule. The final step of N_2O dissociation on Rh(1 1 1) is energetically more stable in which the O atom occupies the 3-fold hollow site, whereas the N_2 molecule occupies the top site, vertically. The adsorption energy of the final product is $E_{ad} = -2.64$ eV.

4. Summary and conclusions

A systematic density functional theory study of the adsorption and dissociation of N_2O on small Rh_{1-6} clusters has been presented. The optimal adsorption site of the N_2O molecule and the relevant magnetic configurations have been determined. In general, the molecular adsorptions on Rh_{1-6} clusters occur with the N_2O molecule binding at bridge sites. Electron charge donation from the Rh_n cluster to the N_2O molecule and the increase of the N–O bond length is observed in all molecularly adsorbed Rh_nN_2O complexes. Dissociative adsorptions of N_2O with small energy barriers are found energetically more favorable for all Rh_n clusters considered. The calculated adsorption energies increase with cluster size ranging from -2.20 eV to -3.28 eV. Interestingly, barrierless dissociative adsorptions are found for the Rh_5 and Rh_6 clusters, however, since the products bind strongly, it is like to poison N_2O decomposition, disabling the capability to form $2N_2$ and O_2 at low temperatures. The less deeper adsorption energies correspond to the smaller Rh_{1-3} clusters, due to a low atom coordination. For the Rh_{4-6} clusters, the molecular precursor states possess a higher magnetic moment than the corresponding dissociative adsorbed states. Rh nanoparticles appear to act hugely more selective than its flat Rh(1 1 1) surface.

Acknowledgements

References

[1] I.S. Parry, A. Kartouzian, S.M. Hamilton, O.P. Balaj, M.K. Beyer, S.R. Mackenzie, J. Phys. Chem. A 117 (2013) 8855–8863.
[2] C. Berg, M. Beyer, U. Achatz, S. Joos, G. Niedner-Schatteburg, V.E. Bondybey, J. Chem. Phys. 108 (1998) 5398–5403.
[3] M.L. Anderson, M.S. Ford, P.J. Derrick, T. Drewello, D.P. Woodruff, S.R. Mackenzie, J. Phys. Chem. A 110 (2006) 10992–11000.
[4] F. Kapteijn, J. Rodriguez-Mirasol, J.A. Moulijn, Appl. Catal. B: Environ. 9 (1996) 25–64.
[5] V. Zhdanov, B. Kasemo, Surface Sci. Rep. 29 (1997) 31–90.
[6] S. Zhao, Y. Ren, W. Lu, Y. Ren, J. Wang, W. Yin, J. Cluster Sci. 23 (2012) 1039–1048.
[7] A.R. Ravishankara, J.S. Daniel, R.W. Portmann, Science 326 (2009) 123–125.
[8] K. Doi, Y.Y. Wu, R. Takeda, A. Matsunami, N. Arai, T. Tagawa, S. Goto, Appl. Catal. B: Environ. 35 (2001) 43–51.
[9] G.E. Marnellos, E.A. Efthimiadis, I.A. Vasalos, Appl. Catal. B: Environ. 46 (2003) 523–539.
[10] F. Mehmood, J. Greeley, P. Zapol, L.A. Curtiss, J. Phys. Chem. B 114 (2010) 14458–14466.
[11] P. Hohenberg, W. Kohn, Phys. Rev. 136 (1964) B864–B871.
[12] G. Kresse, J. Furthmüller, Phys. Rev. B 54 (1996) 11169–11186.
[13] G. Kresse, J. Hafner, Phys. Rev. B 47 (1993) 558–561.
[14] J.P. Perdew, K. Burke, M. Ernzerhof, Phys. Rev. Lett. 77 (1996) 3865–3868.
[15] P.E. Blöchl, Phys. Rev. B 50 (1994) 17953–17979.
[16] H.J. Monkhorst, J.D. Pack, Phys. Rev. B 13 (1976) 5188–5192.
[17] A. Eichler, J. Hafner, J. Chem. Phys. 109 (1998) 5585–5595.
[18] L. Köhler, G. Kresse, Phys. Rev. B 70 (2004) 165405.
[19] G. Henkelman, H. Jnsson, J. Chem. Phys. 111 (1999) 7010–7022.
[20] G. Henkelman, A. Arnaldsson, H. Jónsson, Comput. Mater. Sci. 36 (2006) 354–360.
[21] B.V. Reddy, S.K. Nayak, S.N. Khanna, B.K. Rao, P. Jena, Phys. Rev. B 59 (1999) 5214–5222.
[22] J.L.F. Da Silva, M.J. Piotrowski, F. Aguilera-Granja, Phys. Rev. B 86 (2012) 125430.